Applied Surface Science 706 (2025) 163528

Contents lists available at ScienceDirect

Applied Surface Science

journal homepage: www.elsevier.com/locate/apsusc

Full Length Article

Silanized magnetite nanoparticles as an additive for an electric vehicle transmission base fluid (polyalphaolefin 6)

Fátima Mariño [a,b], Óscar Giner-Rajala [a], Enriqueta R. López [a,*], Alfredo Amigo [c], Josefa Fernández [a]

[a] Laboratory of Thermophysical and Tribological Properties, Nafomat Group, Department of Applied Physics, Faculty of Physics, and Institute of Materials (iMATUS), Universidade de Santiago de Compostela 15782 Santiago de Compostela, Spain
[b] School of Engineering, University of the Basque Country UPV/EHU, Plaza Ingeniero Torres Quevedo 1, 48013 Bilbao, Spain
[c] Laboratory of Thermophysical and Surface Properties of Liquids, Department of Applied Physics, Faculty of Physics, Universidade of Santiago de Compostela 15782 Santiago de Compostela, Spain

ARTICLE INFO

Keywords:
e-transmission fluid
Nanoadditives
Tribological mechanisms
Functionalization
Nanoparticle coating

ABSTRACT

This study aims to examine the effect of particle size on stability and tribological performance of two iron oxide nanoparticles (Fe_3O_4 NPs), with diameters of 14 and 19 nm respectively, modified with octadecyltrichlorosilane, OTS, as lubricant additive in a polyalphaolefin (PAO6) at three concentrations (0.007, 0.015, 0.030 wt%). From the temporal evolution of the refractive index, it can be inferred that the stability times of the nanodispersions containing silanized nanoparticles are longer than those of their uncoated counterparts, increasing with NPs size. The optimal concentration for both nanoparticle sizes was 0.015 wt%. The PAO6 + 0.015 wt% Fe_3O_4-OTS (19 nm) nanodispersion led to wear reductions of up to 59 % (longitudinal sectional area), compared to that of PAO6. The tribological mechanism likely involves the formation of a tribofilm and the mending effect. Measurements of density and three transport properties of nanolubricants at the optimum concentration show no significant variation compared to those of PAO6.

1. Introduction

It is well known that electric vehicles (EVs) are an alternative to reduce the negative environmental impact of traditional internal combustion vehicles. EVs will become the majority mode of transportation in the near future due to rapid evolution of technology, cost reductions, the introduction of new CO_2 emission regulations, and investments and incentives from several governments. A substantial number of automotive manufacturers have adopted the integrated powertrain configuration, in which the electric motor, power electronics, gears and bearings are all in the same block (electrified powertrain or integrated drive-unit). The current generated by the motor causes damage in the bearings and gears, and the high temperatures diminish the lubricant film [1]. The EV transmission fluid (e-fluid or ETF) must fulfill two basic functions: to lubricate the gears and bearings and to cool the electronic components and the motor [1]. High speeds of around 20000 rpm can be achieved by the electric motors used in EVs [2]. For high-speed gears, low viscosity lubricants are more appropriate. Furthermore, reducing oil viscosity reduces viscous heating and increases heat transfer. Hence, e-fluids must be low viscosity oils with high thermal conductivity and adequate electrical properties [2]. These fluids must also have excellent tribological properties and compatibility with materials like copper and polymers. The electrical conductivity values, κ, should be in the static dissipative range (10 to 10^8) pS m^{-1} [3]. An oil with high electrical conductivity ($\kappa > 10^8$ pS m^{-1}) is in the conductive range and does not protect against stray currents. However, if the electrical conductivity of the oil is too low (insulating range, $\kappa < 10$ pS m^{-1}), static charges can build up and discharge in the form of arcs, which can damage or even destroy sensitive components [4]. Base oils are usually insulating, requiring the use of additives to increase the electrical conductivity to the dissipative range.

On the other hand, the rapid expansion of the EV market is intensifying the necessity for the development of this type of fluids, and, in this process, additives play a key role in reducing tribological interface wear and modulating electrical conductivity. Currently, ultra-low viscosity fluids developed for automatic transmissions (ATFs) of internal combustion engine vehicles are used as e-fluids. ATFs include an additive for clutch friction durability. As the EVs do not have clutch, this additive is

* Corresponding author.
E-mail address: enriqueta.lopez@usc.es (E.R. López).

https://doi.org/10.1016/j.apsusc.2025.163528
Received 25 March 2025; Received in revised form 13 May 2025; Accepted 13 May 2025
Available online 14 May 2025

not needed [5]. Hence, it is necessary to develop e-fluids specifically formulated for electrified powertrains. Hydrocarbons such as polyalphaolefins, PAOs, are being used as base oils of e-fluids, which could provide better thermal management compared to water-glycol indirect cooling methods [6]. In this work, a polyalphaolefin of low viscosity, PAO6, has been chosen as base oil. In addition to its low volatility and particularly good oxidative and corrosion stabilities [7], the high viscosity index of this base fluid ensures film protection at high temperatures.

However, reducing the viscosity of the lubricant causes a change from full film lubrication to boundary lubrication [8], increasing friction and wear. Under boundary lubrication conditions, one of the most effective ways to reduce friction and wear is to use additives. Among the novel additives emerged recently, nanoadditives have attracted significant interest due to their unique properties [8]. Thus, different categories of nanoadditives have been explored, including metals and their oxides [9]. Among them, magnetite nanoparticles (Fe_3O_4 NPs) are iron oxide NPs with a wide variety of technical purposes, including applications in the medical, biosensing, memory storage devices and magnetic separation fields, as well as in catalytic processes and energy applications [10–12]. These NPs have also been analyzed as antifriction and antiwear additives of lubricating oils [13–19]. As e-fluids are low viscous, antiwear additives are needed. The most distinctive characteristic of Fe_3O_4 NPs dispersed in a fluid is their magnetic behavior. Thus, when an external magnetic field is applied to the dispersion, these NPs become magnetized, conferring unique properties and advantages to the fluid [13,20]. When these NPs are used as additives of a lubricant, this magnetic nanolubricant can: (a) be retained on the contact area, increasing the lubrication and reducing the amount of fluid required [21]; (b) be trapped, preventing leakage and environmental contamination [20]; and (c) improve tribological properties in comparison with the base oil [20].

Several authors studied the tribological properties of Fe_3O_4 NPs as additives of base oils, in most cases with oleic acid (OA) as dispersant or modifying agent to enhance the dispersibility of the NPs [13,15–19]. Regarding PAO + Fe_3O_4 NPs nanodispersions, de Oliveira et al. [13] evaluated the addition of this kind of NPs (11 nm) at concentrations from 0.4 wt% to 1.6 wt%, dispersed into PAO8 base oil with OA as dispersant, obtaining nanolubricants with high load carrying capacity, good friction reduction and up to 27 % wear rate reduction. Zuin et al. [14] studied Fe_3O_4 NPs (10 nm) coated with stearic acid (SA) also in PAO8, finding that for a concentration of 6.7 wt% of NPs the wear volume decreased by 68 % at 80 °C and 86 % at 230 °C. Moreover, Huang et al. [15] dispersed spherical Fe_3O_4 NPs (13 nm) in PAO4 with the aid of two surfactants (OA and a polyisobutylene succinimide). The optimal NP concentration was found to be 4 wt%, which resulted in a 28 % reduction in the coefficient of friction (CoF). Most authors do not provide the stability times of the nanodispersions, only de Oliveira et al. [13] address this point, finding by visual observation that no noticeable sedimentation was detected, even after 24 h of synthesis. These authors also evaluate the stability of the nanodispersions measuring the UV–Vis spectra over time. In this case, de Oliveira et al. [13] measure the absorbance of the nanolubricants after sonication and one week later, observing that it decreases over time.

Other authors used Fe_3O_4-OA NPs (6.3 and 10 nm) as additives of ester oils [16,17] and of a paraffinic oil [18]. Besides, Gao et al. [19] analyzed the tribological properties of an engine oil containing Fe_3O_4-OA NPs with different morphologies (hexagonal, octahedral, and irregular), all with sizes around 50 nm. Taking into consideration that in almost all the aforementioned articles [13,15–19], OA is the modifying agent or the dispersant of the NPs, it would be interesting to consider other agents such as amines or silanes, for which, up to our knowledge, no studies have been published. In this work, the effect of the size of two commercial Fe_3O_4 NPs modified with a silane, octadecyltrichlorosilane (OTS), on the tribological properties, density, and viscosity of PAO6 dispersions is analyzed. In addition, the thermal and electrical conductivities were measured for PAO6 and the two nanodispersions that have the best tribological properties. The worn surfaces were analyzed using a confocal Raman microscope and a 3D optical profilometer to identify the NPs tribological mechanisms.

2. Materials and methods

2.1. Materials

PAO6 provided by Repsol has a density at 293.15 K of 0.8238 g cm^{-3}, a kinematic viscosity at 373.15 K of 5.84 cSt and a viscosity index of 137.6. Two commercial uncoated Fe_3O_4 NPs with purities of 99.9 % and 99 % and claimed mean diameters of 8 nm and 20–30 nm, respectively, were provided by US Research Nanomaterials, Inc. The OTS used as a modifying agent was purchased from Sigma-Aldrich (purity ≥ 90 %). No further purifications were conducted.

2.2. Functionalization of nanoparticles

The functionalization reaction was performed in accordance with the following procedure: 400 mg of OTS was dissolved in 50 mL distilled water in a round bottom flask using an ultrasonic bath for five minutes to obtain a homogeneous and well dispersed white solution (Fig. 1a and b). Subsequently, 200 mg of Fe_3O_4 NPs (Fig. 1c) were added to the solution, which was then subjected to sonication (frequency: 37 kHz, effective power: 180 W) for 30 min, without allowing the temperature of the bath to exceed 50 °C. During the sonication process, the color of the dispersion undergoes a change from a white-red hue to a deep red, indicative of the reaction between the white OTS and the Fe_3O_4 NPs. After the sonication, the round-bottom-flask is heated to 40 °C on a magnetic hot plate at 400 rpm for 3 h (Fig. 1d–f). Subsequently, the OTS modified Fe_3O_4 NPs (Fe_3O_4-OTS) were washed through sequential centrifugation steps with water, ethanol, and hexane. In each step, 40 mL of solvent were added, and the suspension was centrifugated at 6000 rpm for 10 min. With water, hydrophilic by-products were removed, with ethanol, unreacted OTS and polar organics, and with hexane, nonpolar organic residues. Finally, the NPs (Fig. 1f) were dried using a stove.

2.3. Preparation of the nanolubricants

Nanolubricants of Fe_3O_4-OTS and Fe_3O_4 NPs in PAO6 were prepared. The NP concentrations of the studied dispersions were 0.007 wt%, 0.015 wt% and 0.030 wt%. The nanodispersions were prepared using the two-step method. The dispersions were homogenized first with an ultrasonic probe (50 % amplitude, pulsation off) for 10 min, and then with an ultrasonic bath for 4 h. The temperature of the water bath was controlled to avoid overheating.

Two techniques were used to evaluate the stability of the nanodispersions: photographing and measuring their refractive index, as previously described by Guimarey et al. [22]. Thus, for this last task, a Mettler Toledo refractometer model RA-510M with an expanded ($k = 2$) uncertainty of $2\ 10^{-5}$ was used. As regards visual control method, Azman and Samion [23] have compiled the most common methods used for evaluation of dispersion stability of nanolubricants, analyzing their advantages and limitations. These authors conclude that sedimentation method is the most convenient and cost-effective method, although it is time consuming. Nevertheless, the visual control or sedimentation method is a qualitative technique whose major drawback is that it is difficult to observe when the nanoparticles begin to sediment. In contrast the temporal evolution of the refractive index is a quantitative technique. When the NPs settle at the bottom of the container, the refractive index of the nanodispersions changes, so the nanodispersions are considered more stable when the refractive index hardly varies with time.

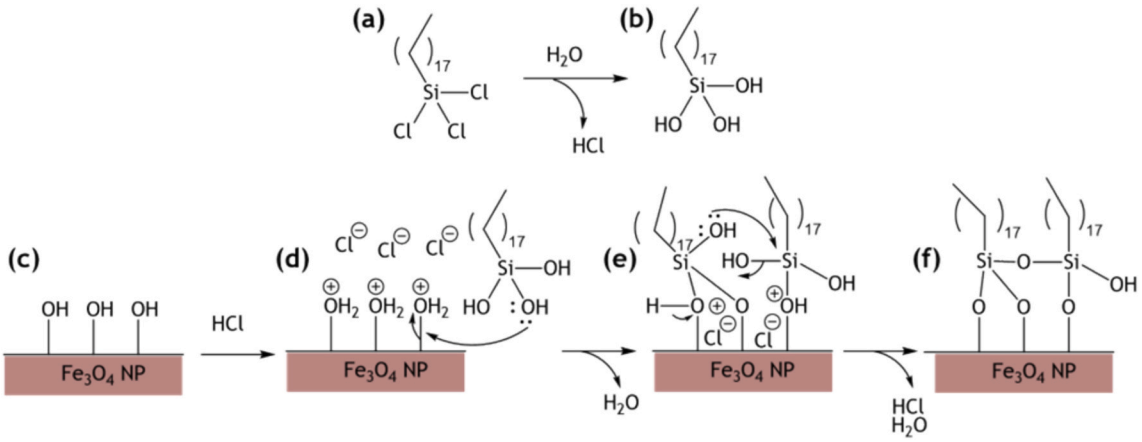

Fig. 1. Functionalization reaction scheme to obtain Fe_3O_4-OTS NPs.

2.4. Tribological properties

A tribological module (T-PTD 200) and a Peltier hood (H-PTD 200) for precise temperature control were connected to an Anton Paar modular rheometer (MCR 302) to measure the friction coefficients (CoF) of steel/steel contacts lubricated with PAO6 or one of the nanodispersions. The contact configuration consisted of a ball (12.7 mm diameter) positioned on three cylindrical pins (both diameter and height of 6 mm). Balls and pins were manufactured from hardened 100Cr6 steel (62–66 Rockwell C hardness). The experiments were conducted using an axial force of 20 N, which corresponds to three normal forces distributed equally at the three pins (9.43 N each one) and a constant angular speed of 213 rpm. The test temperature was 393.15 K, and the sliding distance was 340 m. This temperature value was chosen within the temperature range of a power unit (313–413 K) [24,25], which ensures that the maximum temperature limit of the permanent magnet of the motor (423 K) is not attained. At least three replicates were conducted for each sample, being their average presented together with its standard deviation. Prior to and after the tests, the pins and ball were cleaned with hexane and hot air.

The wear of the tested pins was evaluated using a 3D Sensofar S Neox optical profilometer in confocal mode with a 10x optical lens. Three wear parameters were determined: wear track width (WTW), maximum wear track depth (WTD), and longitudinal sectional area (area). These parameters were calculated as the mean values of nine measurements in the worn track profiles of the nine pins that were tested with each lubricant. The standard deviations of these mean values were then obtained. Finally, to characterize the surface topography, the arithmetic average height (Ra) of the tested pin surfaces was measured.

To compare the tribological performance when using the nanodispersion instead of neat PAO6, the corresponding reductions in X were calculated as

$$X\%reduction = 100\left[\left(X_{PAO6} - X_{nanodispersion}\right)/X_{PAO}\right]$$

where X refers to friction coefficient, wear parameter or roughness values.

2.5. Thermophysical and transport properties

The density and viscosity of PAO6 and of two nanodispersions were measured from 278.15 to 373.15 K with an Anton Paar Stabinger SVM3000 viscosimeter. This apparatus enables the simultaneous and independent measurement of density (ρ) and dynamic viscosity (η) as well as the automatic determination of viscosity index (VI). The apparatus consists in a rotational viscosimeter with cylindrical geometry and a density measurement cell based on the oscillation U-tube principle. The temperature within the cell is controlled by means of a thermostat with cascaded Peltier elements, being measured through a Pt100 thermoresistor with an expanded uncertainty (k = 2) of 0.02 K. The density expanded uncertainty (k = 2) is 0.0005 g cm^{-3} and the expanded uncertainty of dynamic viscosity (k = 2) is 1 %. Viscosity index is determined in accordance with the ASTM D2270 standard with an estimated uncertainty of 2.7 (k = 2).

Thermal conductivities (λ) were measured with an accuracy of around 10 % using a Tempos thermal properties analyzer (METER Group, USA) between 293 and 333 K. This device is based on the transient hot wire method. Five measurements were conducted for each fluid and condition, and the thermal conductivity value is reported as the mean value with its standard deviation.

An Emcee 1153 digital conductivity meter (Emcee Electronics, Inc., USA) covering the range 2–2000 pS m^{-1} was used to determine the electrical conductivities (κ) at temperatures ranging from 298 to 373 K. The conductivity meter verifies the ASTM Standard Test Method D2624 and provides κ values with an accuracy of 10 %. At least five replicates were conducted for each fluid and condition.

3. Results and discussion

3.1. Characterization of nanoparticles

To verify the information given by the manufacturer of the uncoated NPs, US Research Nanomaterials Inc., high-resolution images were taken using a transmission electron microscope (JEOL JEM-1011) to analyze the morphology and determine the NP size (Fig. 2). The two selected nanoparticles have quasi-spherical morphology. TEM images were analyzed with the software ImageJ (version 1.50i, National Institutes of Health, USA), measuring 80–130 NPs. To calculate both average diameters, the data were fitted to obtain the distribution functions (Fig. 2). For the smallest NPs (Fig. 2a) the obtained mean diameter value was 14 nm, with the highest relative frequencies between 12 and 15 nm. On the other hand, the biggest commercial NPs (Fig. 2b) showed a mean diameter value of 19 nm, the highest percentual relative frequency was around 16 nm. As expected, the relative frequencies for larger diameters (21–43 nm) of these NPs were higher than for the smallest Fe_3O_4 NPs. Consequently, from now on, the Fe_3O_4 NPs are identified as Fe_3O_4 (14 nm) and Fe_3O_4 (19 nm) based on their average diameters by TEM. The same nomenclature will be used by the corresponding OTS coated NPs: Fe_3O_4-OTS (14 nm) and Fe_3O_4-OTS (19 nm).

One of the techniques used to confirm the effectiveness of the OTS modification of the Fe_3O_4 NPs is the thermogravimetric analysis (TGA) of the dry modified NPs (Fig. 3). This experiment enables the determination of the degradation temperature of the organic silane coating on the Fe_3O_4 NPs, and the mass of each component (OTS and Fe_3O_4 NPs).

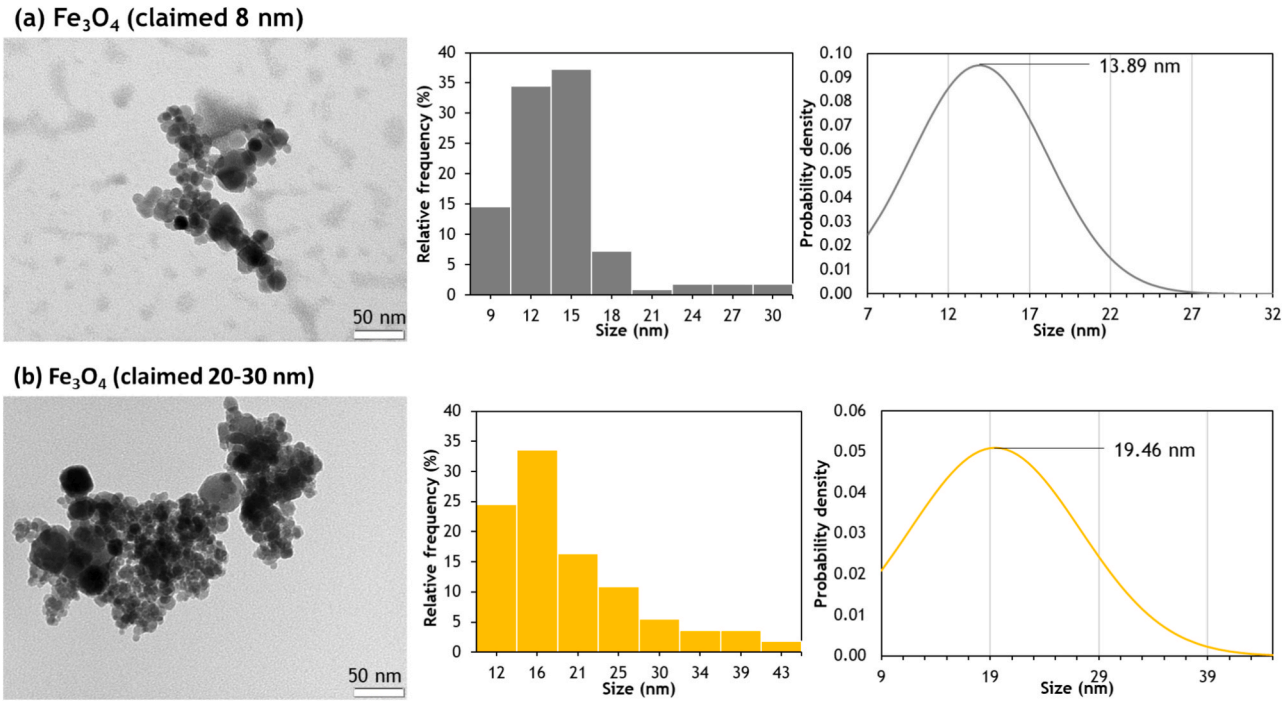

Fig. 2. TEM, histogram, and distribution function of both commercial Fe_3O_4 NPs: (a) Fe_3O_4 (14 nm) and (b) Fe_3O_4 (19 nm).

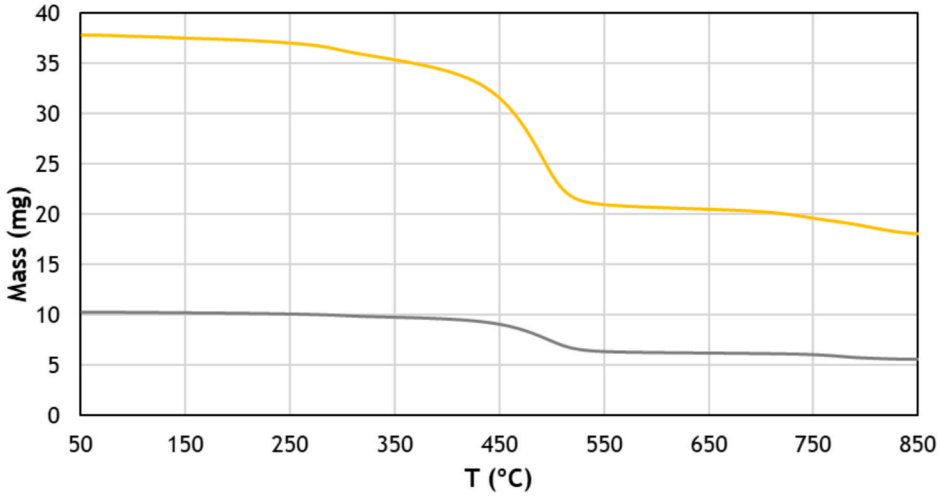

Fig. 3. TGA of the Fe_3O_4-OTS NPs of 19 nm (yellow) and 14 nm (grey).

From experimental data, it is possible to obtain the coupling density of OTS molecules per Fe_3O_4 nanoparticle as well as per nm^2 of NP surface. For both coated NPs, the thermal degradation of the OTS coating started at about 350 °C and continued up to 550 °C, with the remaining mass being uncoated Fe_3O_4 NPs. The TGA indicated that the content of OTS in the nanoparticles was 41 and 46 wt%, respectively, for Fe_3O_4-OTS NPs (14 nm) and Fe_3O_4-OTS NPs (19 nm). The molecular weight of the OTS bound to the NP surface can be utilized to calculate the total number of OTS molecules attached. The density of Fe_3O_4 NPs (5.17 g cm^{-3}) and the average volume of individual NPs are used to estimate the mass of a single NP, which subsequently allows for the determination of the total number of Fe_3O_4 NPs based on the overall sample mass. Assuming a spherical morphology and using the mean NP diameter, the volume of an individual NP is calculated. The ratio of the total number of bound OTS molecules to the total number of NPs yields the number of OTS molecules per NP. Furthermore, dividing this value by the surface area of a single nanoparticle provides the grafting density. Thus, the grafting density, calculated considering the mean diameter values of the NPs, are around 18 OTS molecules per nm^2 of Fe_3O_4 (14 nm) NP and 31 OTS molecules per nm^2 of Fe_3O_4 (19 nm) NP.

Another technique used to verify the effectiveness of the functionalization reaction was Fourier-transform infrared spectroscopy, FTIR. The FTIR spectra of the commercial Fe_3O_4 NPs, OTS and modified Fe_3O_4-OTS NPs of both sizes are shown in Fig. 4, being the main signals identified in Table 1. The FTIR spectra of Fe_3O_4-OTS NPs of both sizes show identical signals coming from Fe_3O_4 and OTS. These include a weak broad band at 3300 cm^{-1} corresponding to a Si–OH stretching vibration [26], and another band at 887 cm^{-1} also originated from the same Si–OH vibration mode [26]. Notably, as expected, in the FTIR of OTS these bands are absent. During the hydroxyl substitution of chloride in OTS (Fig. 1a-b), Si–OH bonds are formed, and the spectra of the coated NPs show that some of the alkoxysilanes of the coating have OH

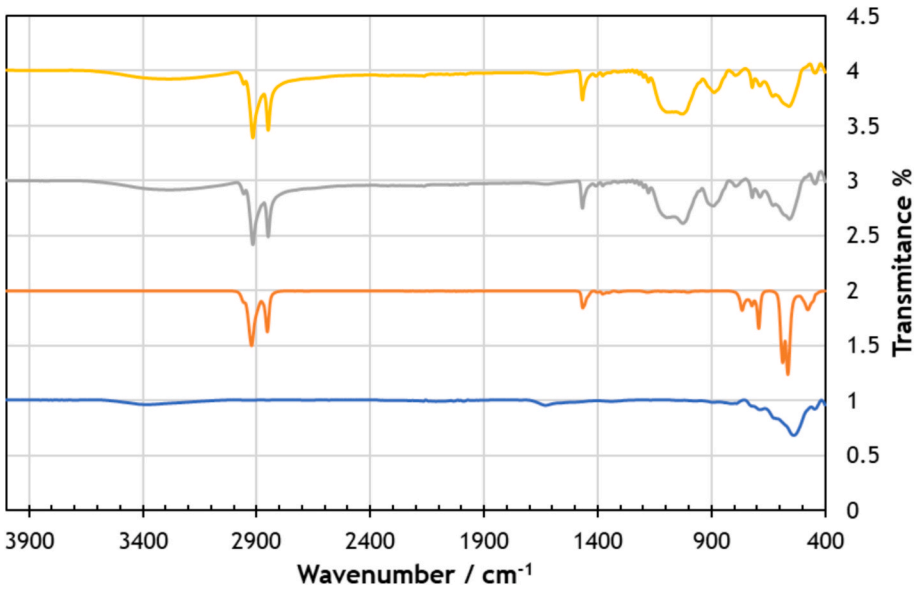

Fig. 4. FTIR spectra of commercial Fe_3O_4 NPs (blue), OTS (orange) and modified Fe_3O_4-OTS NPs grey (14 nm) and yellow (19 nm). The main bands and peaks are identified in Table 1.

Table 1
FTIR spectra: wavenumber and vibration mode assigned to each chemical bond.

Substance	Peak (cm^{-1})	Vibration mode		Chemical bond
Fe_3O_4	626, 563	ν	Stretching	Fe–O
(14 or 19 nm)	443	δ	Torsion	Fe–O
OTS	2962	ν_s	Symmetric stretching	C–H bond in $–CH_3$
	2921	ν_{as}	Anti-symmetric stretching	C–H bond in $–CH_2$
	2852	ν_s	Symmetric stretching	C–H bond in $–CH_2$
	1465	δ_{ip}	In-plane bending	C–H bond in $–CH_2$
	763, 719, 690	ν	Stretching	Si–C
	586, 563	ν_{as}	Asymmetric stretching	Si–Cl bond in $–SiCl_3$
	474	ν_s	Symmetric stretching	Si–Cl bond in $–SiCl_3$
Fe_3O_4-OTS	3300	ν	Stretching	Si–OH
(14 or 19 nm)	2954	ν_s	Symmetric stretching	C–H bond in $–CH_3$
	2915	ν_{as}	Anti-symmetric stretching	C–H bond in $–CH_2$
	2848	ν_s	Symmetric stretching	C–H bond in $–CH_2$
	1465	δ_{ip}	In-plane bending	C–H bond in $–CH_2$
	1095, 1018	ν	Stretching	Si–O–Si
	887	ν	Stretching	Si–OH
	788, 719, 680	ν	Stretching	Si–C
	626, 555	ν	Stretching	Fe–O
	441	δ	Torsion	Fe–O

groups, which had not reacted (Fig. 1d). In addition, two symmetric stretching peaks at 2954 and 2848 cm^{-1}, corresponding to C–H bonds in $–CH_3$ and $–CH_2$ [27,28], as well as an anti-symmetric stretching peak at 2915 cm^{-1} from $–CH_2$ [29], are all attributed to the OTS coating. Furthermore, a peak at 1465 cm^{-1} is observed in both OTS and Fe_3O_4-OTS NPs due to the in-plane bending of C–H bond of $–CH_2$ [29]. In contrast, a band formed by two signals at 1095 and 1018 cm^{-1}, corresponding to Si–O–Si stretching vibrations [30] only appears in the Fe_3O_4-OTS NPs. This further supports the hypothesis that the hydroxyl substitution of chlorides occurs (Fig. 1a and b), as well as the reactions between the coating chains (Fig. 1e and f). The last stretching peaks observed in both OTS and Fe_3O_4-OTS NPs spectra at 788, 719 and 680 cm^{-1} are attributed to Si–C bonds [31]. The remaining peaks of OTS are not observed in the Fe_3O_4-OTS NPs due to the presence of a broad band formed by peaks at 626 and 555 cm^{-1} from the Fe_3O_4 NPs, which corresponds to Fe–O stretching vibrations [32]. The peak with the lowest wavenumber observed in the Fe_3O_4-OTS NPs FTIR spectra at 441 cm^{-1} is from the Fe–O torsional vibration of the Fe_3O_4 NPs (443 cm^{-1}) [33] and not from the Si–Cl symmetric stretching vibration that appears in the OTS spectrum (474 cm^{-1}) [26].

The Fe_3O_4 NP surface silanization process consists of two competing chemical process which give rise to the formation on the NP surface (core) of a complex structure (shell): 1) the formation of Si–O–Fe covalent bonds on the NP surface and 2) the oligomerization among OTS molecules [34]. The band corresponding to the Si–O–Fe covalent bonds cannot be observed in the FTIR spectra of the salinized NPs because appeared at around 584 cm^{-1} and overlaps with the Fe–O vibration of magnetite nanoparticles [35,36]. Nevertheless, in the spectra of silanized NPs, around 584 cm^{-1} the band widens and shows a bend, indicating this overlap. The silane presence is also confirmed by the peaks in the silanized Fe_3O_4 NPs spectra corresponding to Si–O–Si and Si–OH stretching vibrations, as we have previously pointed out.

Fig. 5 depicts the Raman spectra of OTS, uncoated Fe_3O_4 NPs, and Fe_3O_4-OTS NPs. As can be observed, the spectra of both coated NPs exhibit the main characteristic bands of the spectra of OTS and of uncoated Fe_3O_4 NPs. Therefore, it can be observed a strong band around

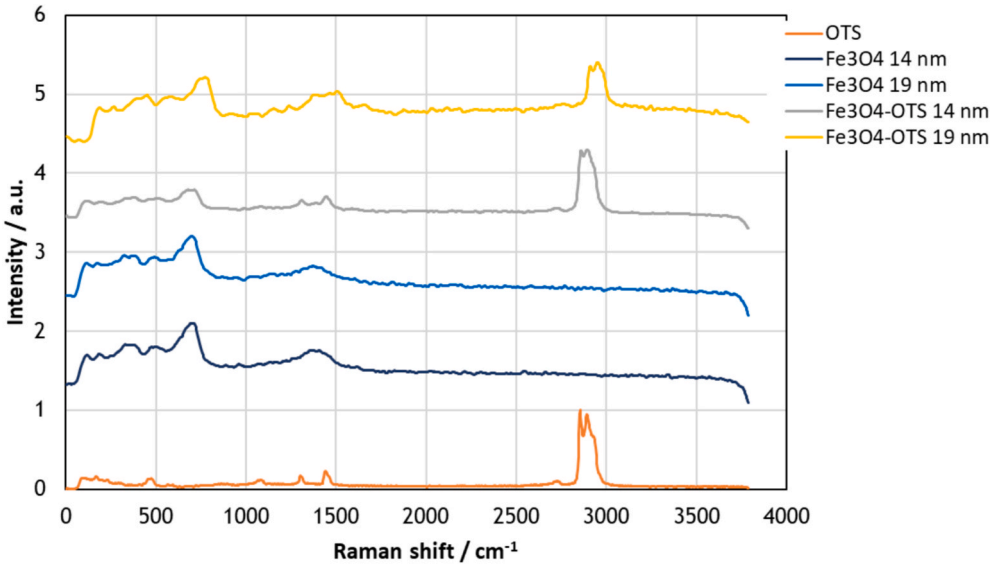

Fig. 5. Raman spectra of commercial Fe_3O_4 NPs (dark blue: 14 nm; light blue: 19 nm), OTS (orange) and modified Fe_3O_4-OTS NPs: grey (14 nm) and yellow (19 nm).

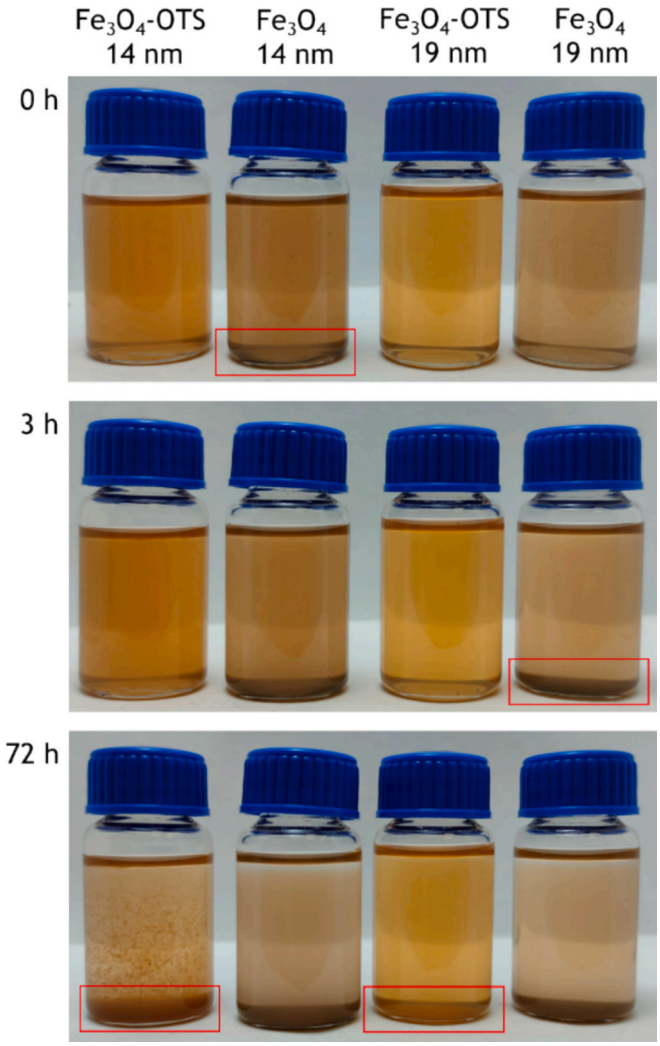

Fig. 6. Photographs of 0.015 wt% nanodispersions of Fe_3O_4-OTS and Fe_3O_4 NPs of two sizes in PAO6.

668 cm^{-1} coming from Fe–O symmetric stretching [31], accompanied by weaker bands at 311–380 cm^{-1} which are ascribed to Fe–O symmetric bending [37], in uncoated Fe_3O_4 NPs, and the band at 2922 cm^{-1}, resulting from the C–H stretching of the $–CH_2$ [38,39] in OTS.

3.2. Stability of the nanolubricants

Once the nanodispersions were prepared, the stability of PAO6 + 0.015 wt% Fe_3O_4 NPs and PAO6 + 0.015 wt% Fe_3O_4-OTS NPs with NPs of both average diameters (14 nm and 19 nm) was evaluated using two methods: sediment photo capturing (Fig. 6) and the evolution of the refractive index (Fig. 7). The results obtained from both methods exhibited a similar stability trend for the four nanodispersions, with the least stable nanodispersion being that of the uncoated Fe_3O_4 NPs of 14 nm, followed by that of the other commercial Fe_3O_4 NPs (19 nm). Similarly, the nanodispersion of OTS modified NPs of 19 nm are more stable than their 14 nm counterpart. The stability trend can be summarized as follows: Fe_3O_4 NPs (14 nm) < Fe_3O_4 NPs (19 nm) < Fe_3O_4-OTS NPs (14 nm) < Fe_3O_4-OTS NPs (19 nm). Specifically, from the analysis of the refractive index results in Fig. 7, it can be inferred that 24 h after the preparation of the nanodispersions containing Fe_3O_4-OTS NPs, their refractive index increased by 0.06 % in the case of the one containing the smallest nanoparticles (14 nm) and 0.03 % for the one containing the nanoparticles with the largest average diameter (19 nm). These results indicate that both nanodispersions are relatively stable during this period and are in agreement with previous literature results [34,40] about the silanization of NPs, which indicate that the greater curvature of small NPs limits the reaction of the alkoxysilane with the NPs (Fig. 1d and e), potentially leading to lower grafting densities and, therefore, poorer stability times. Thus, increasing the Fe_3O_4-OTS NP radius (larger NPs have less curvature) decreases the steric hindrance effects and consequently increases the grafting density of OTS, which increases the packing between the grafted chains and promotes steric stabilization [34,40], and better dispersion stability in PAO6, reducing aggregation. This hypothesis is consistent with the grafting densities obtained, which are 18 molecules of OTS per nm^2 for the Fe_3O_4-OTS (14 nm) NPs and 31 molecules of OTS per nm^2 for the Fe_3O_4-OTS (19 nm) NPs, the latter showing slightly better stability times in PAO6 (Figs. 6 and 7). These findings are also consistent with literature results where oleic acid functionalized Fe_3O_4 NPs (Fe_3O_4-OA) were tested as additives in two ester base oils [16,17]. In the first article [16], a one-step method was used to separately disperse NPs of two sizes (6.3 nm and 10 nm) at

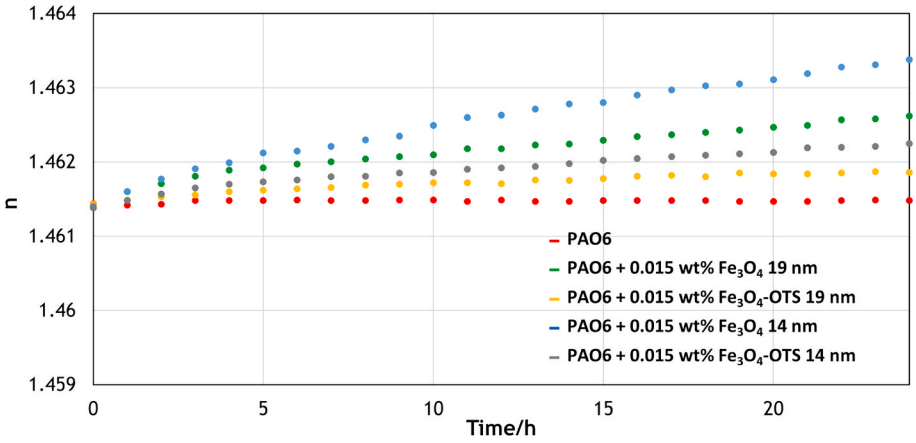

Fig. 7. Evolution over 24 h of the refractive index at 298.15 K of PAO6 and its nanodispersions at concentrations of 0.015 wt% Fe_3O_4-OTS and Fe_3O_4 NPs of two sizes. The expanded (k = 2) uncertainty of the data is 2 10^{-5}.

0.015 wt% in trimethylolpropane trioleate (TMPTO) base oil. Stabilitiy times longer than eleven months were obtained with both nanodispersions. The grafting density in this case were 5 and 6 oleic acid molecules per NP surface area in nm^2 for the NPs of 6.3 nm and 10 nm, respectively. In the second work [17], the 6.3 nm diameter Fe_3O_4-OA NPs were tested as additives in other ester oil, tris(2-ethylhexyl) trimellitate (TOTM), at different concentrations. Two weeks after its preparation by the two-step method, the nanodispersion containing 0.015 wt% of NPs showed signs of sedimentation. Thus, the method used to prepare the nanodispersions and the nature of both the base oil and the coating seems to be the key factors to find long-term stabilities rather than only the grafting density, which is higher, by nm^2, in the present work whereas 72 h after their preparation, the two nanodispersions studied in the present work show precipitation.

The 0.015 wt% Fe_3O_4-OTS NPs concentration nanodispersion has been chosen to analyze the stability because it is the concentration of greatest interest because it is the optimal concentration from a tribological point of view. If the NP concentration is higher, the inter-particle distance will be smaller, which in turn increases the van der Waals attractive forces that favor their aggregation [23].

A fresh aliquot of each nanodispersion was used to measure each property. For the measurement of the transport properties, the nanodispersions were sonicated daily under the same conditions as they were prepared. The effects of the temperature and of resuspension of the NPs in the nanodispersion were not evaluated.

3.3. Tribological results

The results of the ball-on-three-pins friction tests are summarized in Table 2 and Fig. 8. All nanolubricants lead to CoF values slightly lower than PAO6, with the highest reduction of 8 % for PAO6 + 0.015 wt% Fe_3O_4-OTS (14 nm) nanodispersion. Small reductions in CoF and high reductions in wear are common for low-viscosity oils with nanoadditives

Table 2
Average friction coefficient values (CoF) at 393.15 K and their standard deviations (σ) for PAO6 base oil and its Fe_3O_4-OTS nanodispersions with different weight percentages (wt%).

	CoF	σ	Reduction (%)
PAO6	0.1542	0.0026	
+ 0.007 wt% Fe_3O_4-OTS (14 nm)	0.1512	0.0019	2.0
+ 0.015 wt% Fe_3O_4-OTS (14 nm)	0.1418	0.0014	8.0
+ 0.030 wt% Fe_3O_4-OTS (14 nm)	0.1535	0.0016	0.5
+ 0.007 wt% Fe_3O_4-OTS (19 nm)	0.1535	0.0043	0.4
+ 0.015 wt% Fe_3O_4-OTS (19 nm)	0.1490	0.0023	3.4
+ 0.030 wt% Fe_3O_4-OTS (19 nm)	0.1534	0.0049	0.5

[41–44]. The CoFs of PAO6 + Fe_3O_4-OTS (19 nm) NPs nanolubricants show the same trend than those with Fe_3O_4-OTS (14 nm) NPs, however, the reductions in the coefficient of friction are lower, obtaining a maximum reduction of only 3.4 % with the nanodispersion containing 0.015 wt% Fe_3O_4-OTS.

Wear results are summarized in Table 3. Interestingly, the effect of the size of the nanoparticle in the wear is different than the trend observed in the CoF. The lowest values of the wear parameters are obtained in the pins lubricated with the nanodispersions containing Fe_3O_4-OTS (19 nm) NPs, specifically with the PAO6 + 0.015 wt% Fe_3O_4-OTS (19 nm) NPs nanolubricant with reductions, comparing with PAO6, of 20 %, 41 % and 59 % for WTW, WTD and longitudinal sectional area, respectively. For the smaller nanoparticles, Fe_3O_4-OTS (14 nm) NPs, the highest reductions were also obtained with the dispersions with 0.015 wt% coated NPs being 16 %, 25 % and 42 % for WTW, WTD and longitudinal sectional area. It is noteworthy that the PAO6 + 0.007 wt% Fe_3O_4-OTS (14 nm) exhibited a higher mean WTD value compared to that of the PAO6 base oil, 2.97 μm against 2.60 μm, a 14 % increment. Despite that, the WTW and area mean values are 2 % and 12 % lower than those of the base oil, respectively. In this way, it can be considered as having a positive or neutral effect on wear. The same wear trend with the NPs size was previously found for Fe_3O_4 NPs coated with oleic acid as additives of an ester oil [16].

The superior performance of larger Fe_3O_4-OTS NPs (19 nm) as antiwear additives compared to their smaller counterparts (14 nm) may be attributed to differences in surface functionalization. Given their high specific surface area relative to volume, the physicochemical properties of NPs are predominantly governed by surface characteristics rather than bulk ones. In addition, the number of surface and near-surface atoms is larger as compared to that of bulk atoms [45]. Surface atoms are inherently unstable and highly reactive, rendering then prone to aggregation as a means to reduce surface energy [46]. In the context of dispersions in non-aqueous lubricants composed of low-polar or nonpolar molecules, one of the most effective strategies to mitigate this issue involves the covalent attachment of long nonpolar alkyl chains to the NP surface. To this end, OTS was used as a surface-modifying agent. The resulting Fe_3O_4-OTS hybrid NPs consists of a rigid Fe_3O_4 NP core and a soft organic shell comprising OTS chains covalently bonded to the NP surface, with up to three per OTS molecule. As discussed in Section 3.2, an increase in NP radius leads to a decrease in steric hindrance, thereby allowing a higher grafting density of OTS molecules. This, in turn, enhances steric stabilization and significantly reduces NP aggregation. The lower degree of aggregation in nanodispersions containing larger silanized NPs positively impacts their tribological performance, particularly their antiwear properties rather than the antifriction capabilities [47]. Aggregation restricts the free mobility of NPs and facilitates

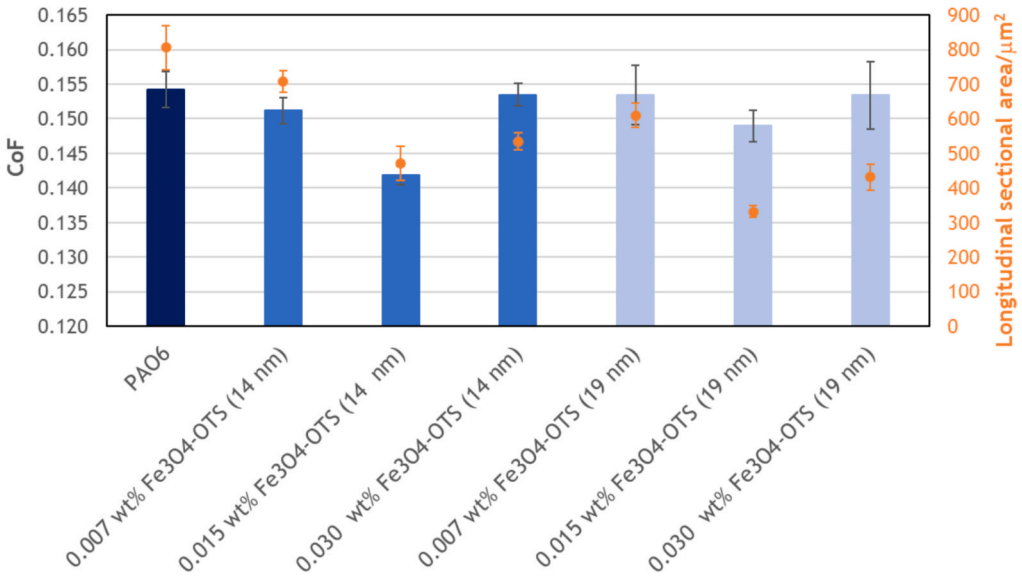

Fig. 8. Average friction coefficient values (CoF, blue) and longitudinal sectional area (orange) for PAO6 and its Fe_3O_4-OTS nanolubricants.

Table 3
Mean values of the wear parameters (width, maximum depth, and longitudinal sectional area) of the wear track (WTW, WTD, and area, respectively) together with their standard deviations (σ) for PAO6 base oil and its nanodispersions with Fe_3O_4-OTS NPs at different weight percentages (wt%).

	WTW/μm	σ/μm	WTD/μm	σ/μm	Area/μm²	σ/μm²
PAO6	435	10	2.60	0.19	806	65
+ 0.007 wt% Fe_3O_4-OTS (14 nm)	427	6	2.97	0.07	708	31
+ 0.015 wt% Fe_3O_4-OTS (14 nm)	364	11	1.96	0.16	471	50
+ 0.030 wt% Fe_3O_4-OTS (14 nm)	378	8	2.15	0.09	535	25
+ 0.007 wt% Fe_3O_4-OTS (19 nm)	408	7	2.39	0.07	610	36
+ 0.015 wt% Fe_3O_4-OTS (19 nm)	350	5	1.55	0.06	332	17
+ 0.030 wt% Fe_3O_4-OTS (19 nm)	360	6	1.80	0.10	431	37

their expulsion from frictional interfaces, thereby hindering their ability to penetrate surface asperities or interfacial gaps within tribological contacts [23]. Moreover, the organic shell formed by OTS contributes to the prevention of material transfer and suppresses direct contact and cold-welding between sliding surfaces [47]. As a result, larger Fe_3O_4-OTS NPs exhibit a lower tendency to aggregate, improved dispersion stability over time and enhanced antiwear performance relative to smaller counterparts.

Another parameter that was evaluated to study the effect of nanoparticles on wear is the arithmetic average roughness (Ra) of the worn surfaces of the pins, with a Gaussian filter of 0.25 mm. The results are presented in Fig. 9. The highest Ra value was obtained for the pin lubricated with the PAO6 base oil, 33 % higher than the Ra of the untested pin. The lowest Ra was obtained for the pin lubricated with PAO6 + 0.015 wt% Fe_3O_4-OTS (19 nm). In this last case, reductions of 44 % compared to the untested pin and of 58 % compared to the pin lubricated with PAO6 were achieved. The Ra values significantly varied with the concentration of the Fe_3O_4-OTS (19 nm) NPs. However, the Ra values found with Fe_3O_4-OTS (14 nm) are similar for all the studied concentrations, reducing around 6 % compared to the untested pin and 30 % compared to the pin lubricated with PAO6. This could imply a change in the tribological mechanism with the size of the nanoparticle.

In general, the observed trend in roughness is consistent with the wear data reported in Table 3, as trends for longitudinal sectional areas (Fig. 8) and for Ra (Fig. 9) are similar. This feature is also in accordance with the worn surface topographies of the pins tested with the six nanolubricants (Fig. 10).

Finally, tribological mechanisms were further assessed by confocal Raman microscopy on the worn surface of the pins lubricated with PAO6 [44], PAO6 + 0.015 wt% Fe_3O_4-OTS (14 nm) NPs (Fig. 11) and PAO6 + 0.015 wt% Fe_3O_4-OTS (19 nm) NPs (Fig. 12). The presence of different components on the surface is evidenced by confocal Raman microscopy. Mapping images with the location of each component in a distinct color obtained using Project FIVE software are shown in Figs. 11 and 12. As previously demonstrated [44], the mapping image of the pin lubricated with PAO6 reveals the presence of PAO6, iron oxides, and carbon resulting from the degradation of PAO on the surface. Presence of carbon in the worn surfaces lubricated by neat PAO6 has been previously observed by Ratoi et al. [48]. According to these authors, this presence could be indicative of lubricant degradation due to high local temperatures reached during friction tests or during the Raman analyses themselves. Apart from iron oxides detected on the worn surfaces lubricated by PAO6 [44], it should be noted that oxides have also been identified in the contact area lubricated with other nanolubricants containing PAOs and non-ferrous NPs, but in smaller areas [49,50].

In the case of the worn surface previously lubricated with PAO6 + 0.015 wt% Fe_3O_4-OTS NPs (Fig. 11 for NPs of 14 nm and Fig. 12 of 19 nm), four components are found: Fe_3O_4 (red), coated Fe_3O_4 NPs (sky blue), PAO6 (blue) and carbon (green). In both mappings, the areas corresponding to Fe_3O_4 (red) are the more abundant, followed by the Fe_3O_4-OTS areas (sky blue) and carbon from lubricant degradation (green). It seems clear that part of the signal of Fe_3O_4 comes from oxidation of the rubbing surfaces and part from uncoated Fe_3O_4 NPs. To distinguish between this last signal and that coming from coated Fe_3O_4 NPs, the band at 2922 cm^{-1}, resulting from the C–H stretching of the $–CH_2$ [38,39] was used.

As it was pointed out, it is likely that part of the Raman signal corresponding to iron oxides comes from uncoated Fe_3O_4 NPs due to coating loss of the Fe_3O_4-OTS NPs during tribological testing. In this regard, due to the high temperatures and pressures caused by the

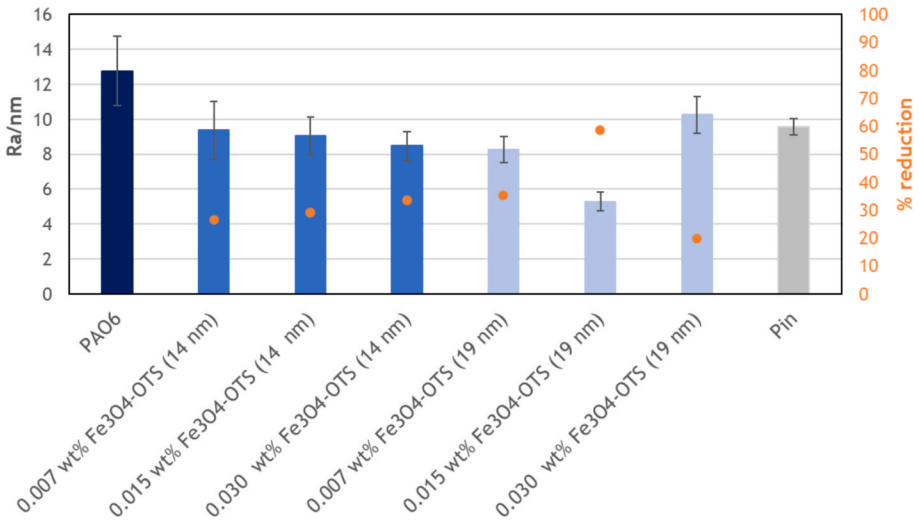

Fig. 9. Mean arithmetic average roughness (Ra) of untested pin surface (gray) and the worn pin surfaces lubricated with PAO6 (navy blue), Fe_3O_4-OTS (14 nm) NP nanodispersions (blue) and Fe_3O_4-OTS (19 nm) NP nanodispersions (light blue).

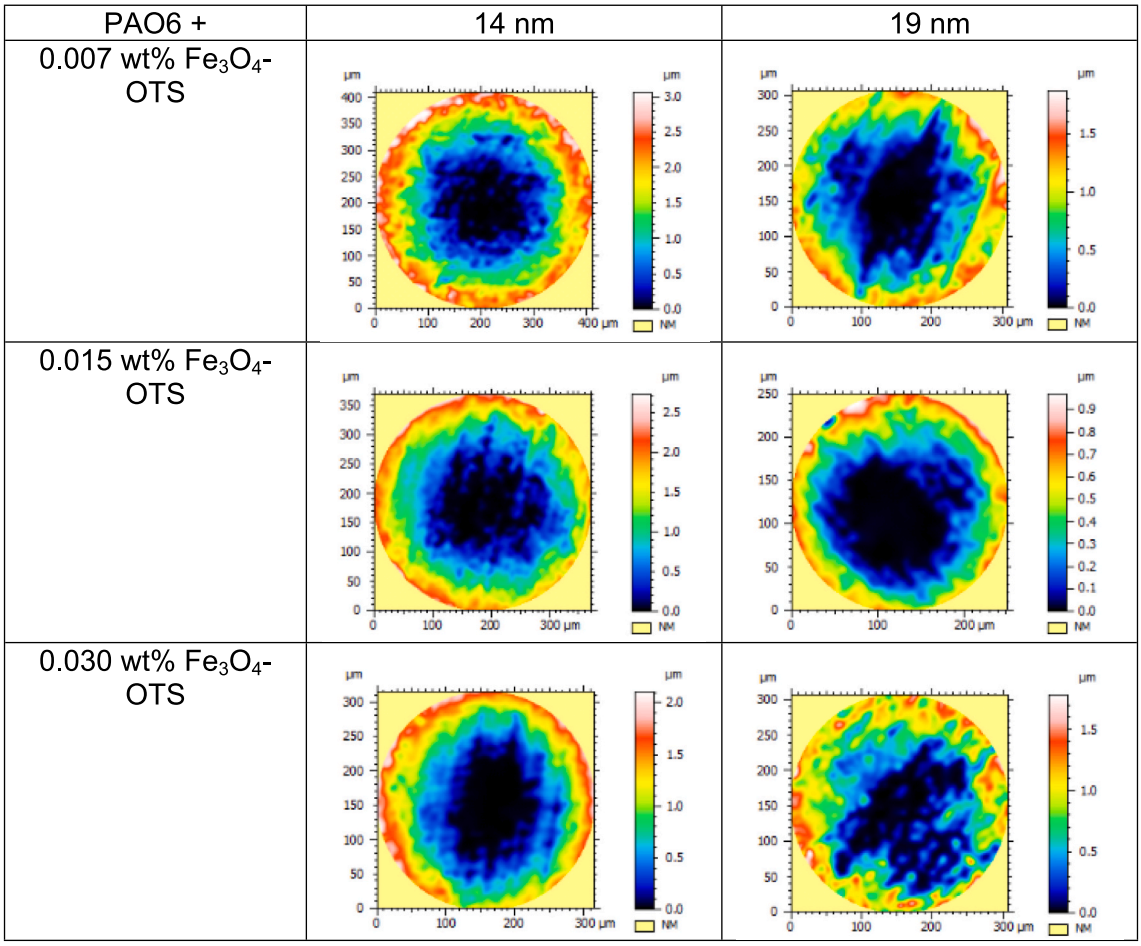

Fig. 10. Worn surface topographies of the pins tested with the six nanolubricants.

friction process, some tribochemical reactions occur. Thus, these conditions cause the breaking of the bonds between OTS and the Fe_3O_4 NPs, similar to what was found by Zhang et al. [51] for SA modified TiO_2 NPs by XPS and Mariño et al. [44] for SA modified SiO_2 NPs by confocal Raman microscopy. The sizes of the red areas in the Raman mappings indicate that the Fe_3O_4-OTS (14 nm) NPs have more tendency to the Fe-O-Si bond breakage on the tribo-contact area which could explain the poorer wear results.

One of the tribological mechanisms taking place is then the tribofilm formation. In our case these tribofilms contain, apart from the coated nanoparticles, iron oxides and amorphous carbon. Presence of lubricious iron oxides NPs is responsible for the better antiwear capability of

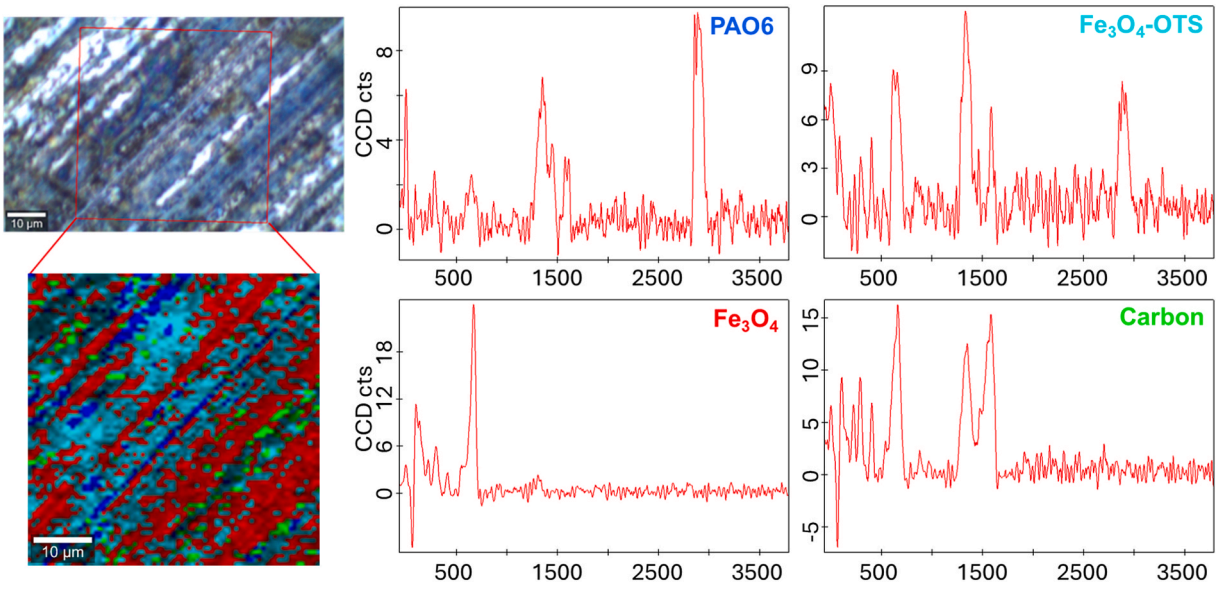

Fig. 11. Raman mapping of the worn pin surface tested with PAO6 + 0.015 wt% Fe_3O_4-OTS (14 nm) NPs and spectra of the components on that surface: uncoated Fe_3O_4 (red areas), Fe_3O_4-OTS (sky blue areas), PAO6 (blue areas) and carbon (green areas).

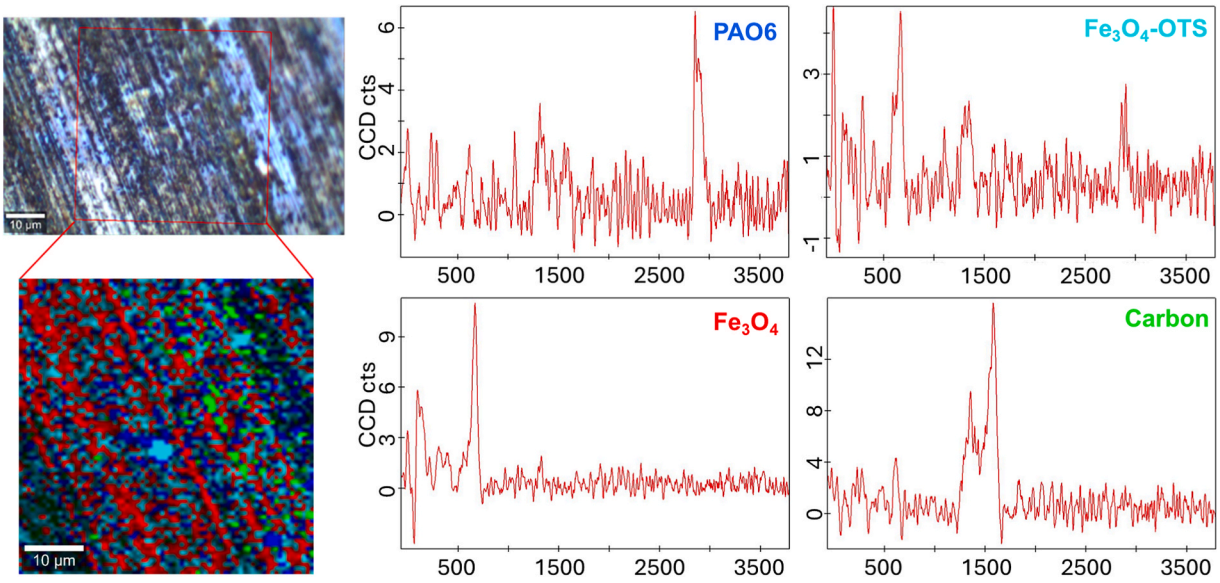

Fig. 12. Raman mapping of the worn pin surface tested with PAO6 + 0.015 wt% Fe_3O_4-OTS (19 nm) NPs and spectra of the components on that surface: Fe_3O_4 (red areas), Fe_3O_4-OTS (sky blue areas), PAO6 (blue areas), carbon (green areas).

nanolubricants. Carbon (green areas) was identified as amorphous carbon because of the presence of the peaks at 1346 cm^{-1} (D band) and 1580 cm^{-1} (G band) [52]. This carbon tribolayer, coming from lubricant degradation, has a positive effect on reducing friction [52]. As the areas in PAO6 mapping and in nanolubricant mappings are comparable, the effect of the formation of carbon tribolayers does not change the anti-friction capability of PAO6 due to degradation when adding the nano-additives. On the other hand, during friction tests, grooves in the sliding direction are created, being clearly visible (Figs. 11 and 12). As can be observed in both mappings, both NPs are located (mainly Fe_3O_4 NPs) following the grooves of the wear, indicating that other tribological mechanism present is mending effect.

3.4. Thermophysical and transport properties

The dynamic viscosity, density, and viscosity index of PAO6 and its dispersions containing 0.015 wt% concentration of Fe_3O_4-OTS NPs of both sizes were measured from 278.15 to 373.15 K. Due to the low concentration used in these nanodispersions, the effect of the nano-additive in these properties is negligible. The density values of nano-dispersions have absolute relative deviations of less than 0.1 % compared to those of the PAO6 base oil (Table 4). These deviations are less than the density uncertainty (around 0.6 %). On the other hand, the maximum increase in dynamic viscosity is 1.1 % with respect to PAO6 (Table 4), which is close to the viscosity uncertainty (1 %). The negligible viscosity increase is satisfactory because in the case of ETFs, low viscosity is required for high-speed gears to avoid viscous heating and decrease the heat transfer, but at the same time a good wear protection is required to address durability issues [53]. Regarding the viscosity index, there is an increase of 0.73 % for the smaller NPs (VI 138.6) and of 0.80 % for the larger NPs (VI 138.7) in comparison with PAO6 (VI 137.6). These increases are less than the VI uncertainty (2.7).

Table 4
Densities (ρ) and dynamic viscosities (η) of PAO6 and its Fe_3O_4-OTS nanolubricants measured at atmospheric pressure. For density, the expanded uncertainty (k = 2) is 0.0005 g cm^{-3} and the expanded uncertainty of dynamic viscosity (k = 2) is 1 %.

Lubricant	PAO6	0.015 wt% Fe_3O_4-OTS (14 nm)	0.015 wt% Fe_3O_4-OTS (19 nm)	PAO6	0.015 wt% Fe_3O_4-OTS (14 nm)	0.015 wt% Fe_3O_4-OTS (19 nm)
T/K	ρ/g cm^{-3}	ρ/g cm^{-3}	ρ/g cm^{-3}	η/mPa s	η/mPa s	η/mPa s
278.15	0.8329	0.8336	0.8328	138	139	139
283.15	0.8298	0.8305	0.8298	103	104	104
288.15	0.8268	0.8275	0.8268	78.2	79.0	78.9
293.15	0.8238	0.8244	0.8237	60.4	61.0	61.0
298.15	0.8207	0.8214	0.8207	47.6	48.1	48.0
303.15	0.8176	0.8183	0.8176	37.7	38.1	38.0
308.15	0.8145	0.8152	0.8146	30.4	30.7	30.7
313.15	0.8114	0.8121	0.8115	24.8	25.1	25.1
318.15	0.8084	0.8090	0.8084	20.5	20.7	20.7
323.15	0.8053	0.8059	0.8054	17.2	17.3	17.3
328.15	0.8021	0.8028	0.8023	14.5	14.6	14.6
333.15	0.7990	0.7997	0.7992	12.4	12.5	12.5
338.15	0.7959	0.7966	0.7961	10.6	10.7	10.7
343.15	0.7928	0.7935	0.7930	9.21	9.28	9.29
348.15	0.7897	0.7903	0.7900	8.04	8.10	8.12
353.15	0.7866	0.7872	0.7868	7.07	7.13	7.14
358.15	0.7834	0.7841	0.7837	6.26	6.31	6.32
363.15	0.7803	0.7809	0.7806	5.58	5.63	5.64
368.15	0.7772	0.7778	0.7775	5.01	5.05	5.06
373.15	0.7740	0.7747	0.7744	4.52	4.56	4.57

Thermal conductivity was measured at three temperatures within the range 293–333 K for PAO6 and the PAO6 + 0.015 wt% Fe_3O_4-OTS (14 nm and 19 nm) nanolubricants (Fig. 13). As expected for non-aqueous systems, the λ values for all the samples decrease slightly with increasing temperature. Slightly higher λ values were achieved for the PAO6 + 0.015 wt% Fe_3O_4-OTS 19 nm nanolubricant than for PAO6. As can be observed, the lower the temperature, the higher the λ improvement, although these improvements are small because of the low mass fraction of nanoadditive. The positive impact of enhanced thermal conductivity on the EV's integrated transmission system is twofold: to avoid a negative impact on motor performance of high temperatures and to protect the power electronics [25,53] However, no enhancements were found with the nanolubricant containing the Fe_3O_4-OTS of 14 nm. Mishra et al. [54] performed a review of the effect of particle size on thermal conductivity of nanofluids. These authors point out that, although it is not usual, several studies have shown improvements in thermal conductivity when the size of the NPs increases. This was explained by the sedimentation associated with the excessive clustering of small NPs [54]. However, for the two Fe_3O_4-OTS nanodispersions, the λ variations are significantly lower than the experimental uncertainties (Fig. 13).

The electrical conductivities (Fig. 14), κ, have been measured in the range 298 to 373 K for PAO6 and the nanodispersions PAO6 + 0.015 wt % Fe_3O_4-OTS (14 nm or 19 nm) NPs. As expected, the κ values for the base oil and the two nanodispersions increase exponentially with temperature, i.e., as the viscosity of the fluid decreases. Nevertheless, the addition of the nanoadditives does not result in a meaningful change of this property, due to the low NP concentration. As indicated, the electrical conductivity of ETFs must fall within the range of the electrically dissipative materials (10 to 10^8 pS m^{-1}). This is the case for all the temperatures analyzed except for those below 313 K (Fig. 14).

In summary, under the present conditions, in general 1) the higher Fe_3O_4-OTS (19 nm) NPs remain more stable in PAO6 and tribologically perform better than Fe_3O_4-OTS (14 nm) and 2) the addition of a small amount (0.015 wt%) of Fe_3O_4-OTS (19 nm) to PAO6 improves the tribological behavior of PAO6, especially the antiwear ability, while the

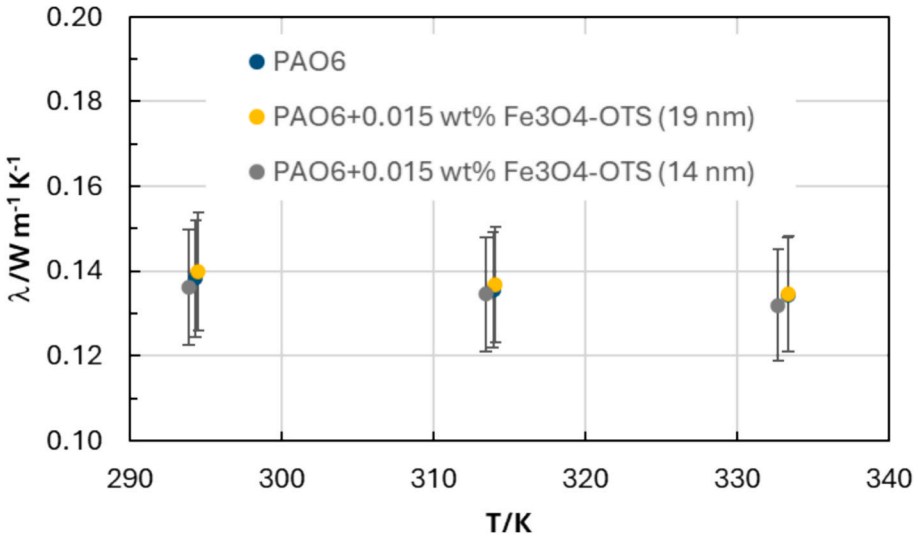

Fig. 13. Average thermal conductivity, λ, as a function of the temperature: PAO6 (blue), PAO6 + 0.015 wt% Fe_3O_4-OTS 14 nm (gray) and PAO6 + 0.015 wt% Fe_3O_4-OTS 19 nm (yellow).

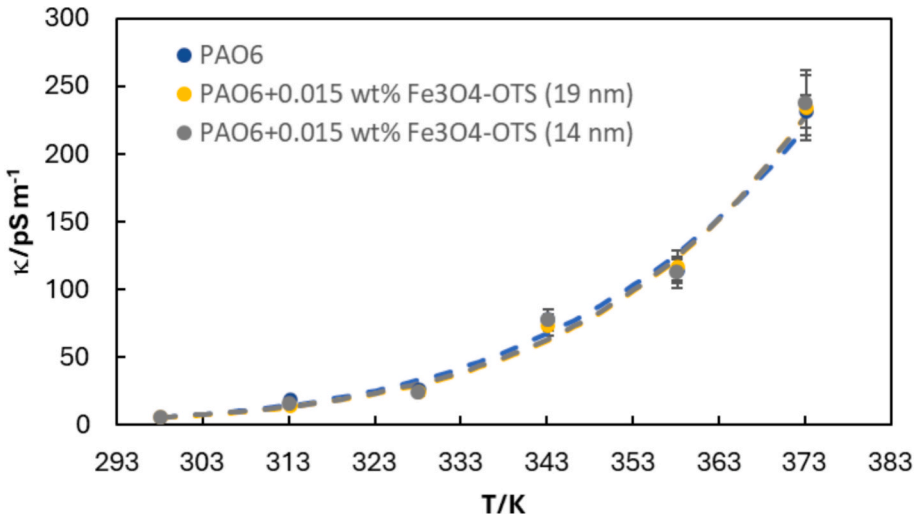

Fig. 14. Average electrical conductivities, κ, as a function of the temperature: PAO6 (blue), PAO6 + 0.015 wt% Fe_3O_4-OTS 14 nm (gray) and PAO6 + 0.015 wt% Fe_3O_4-OTS 19 nm (yellow). Dashed lines represent the Vogel-Fulcher-Tammann correlations [55].

analyzed density and transport properties remain practically unchanged, which is an interesting result from the perspective of an possible application. The main drawback of the present nanodispersions is the low stability time, which limits their applicability. Several points could be addressed to try design nanodispersions with long-term stability. Thus, a) the methods of preparing the nanodispersions involving the evaporation of a volatile solvent led to greater stability results compared to the present two-step method [34,47]; b) increasing the size of the core (bare Fe_3O_4 NPs) led to nanodispersions involving Fe_3O_4-OTS nanoadditives that were more stable [34,47]; c) The combined use of other dispersants could improve the stability of the nanodispersions. In this regard, a particularly promising class of dispersants for NPs are ionic liquids (ILs) because they combine excellent dispersing properties and demonstrated to be effective antifriction and antiwear additives [56].

4. Conclusions and scope for future work

In this work, two commercially available Fe_3O_4 NPs of two average particle sizes (14 and 19 nm) were modified with a silane (octadecyltrichlorosilane, OTS) and used as lubricant nanoadditives in PAO6. The main findings and conclusions that can be derived from this study can be summarized as follows:

- Silanization reaction of the commercial Fe_3O_4 NPs was successfully done, as was evidenced by TGA and FTIR analyses. Results of the TGA analysis demonstrated that NPs with a larger average particle size exhibited higher grafting density in comparison to NPs with smaller average particle size.
- Stability of the prepared nanodispersions in PAO6 demonstrated that the Fe_3O_4-OTS (19 nm) had the most favorable dispersibility in the base oil, achieving a stability time of 72 h. Conversely, the two types of commercial Fe_3O_4 NPs exhibited the least favorable results with stability times lower than three hours.
- Optimal NP concentration for friction and wear reductions was 0.015 wt% for both coated nanoparticle sizes. While the CoF values showed slight reductions with the addition of the Fe_3O_4-OTS NPs at all concentrations, the impact on the wear reduction was considerably more pronounced. The 0.015 wt% Fe_3O_4-OTS (19 nm) nanodispersion lead to the most substantial reductions reaching 20, 41 and 59 % (WTW, WTD, longitudinal sectional area).
- Tribological mechanisms were evaluated through Ra and Raman results. From Ra values, it can be inferred that the Fe_3O_4-OTS (19 nm) NPs have a concentration dependent mechanism while the Fe_3O_4-OTS (14 nm) NPs do not show the same trend. Moreover, Raman results indicate that the Fe_3O_4-OTS (14 nm) NPs have more tendency to Fe–O–Si bond breakage on the tribo-contact area which could explain the poorer wear results. It is likely that the tribological mechanisms are tribofilm formation and mending effect.
- Density and transport properties of the 0.015 wt% Fe_3O_4-OTS nanodispersions showed that such a small concentration of nanoparticles does not practically influence viscosity, density, thermal and electrical conductivities, and viscosity index.
- Thus, under the present conditions, the addition of a small quantity (0.015 wt%) of Fe_3O_4-OTS (19 nm) to PAO6 improves the tribological behavior of PAO6, especially the antiwear capability, while the density and the analyzed transport properties remain roughly unaffected.

Finally, we must point out that this is a fundamental study, the ultimate goal of which is to contribute to the creation of a critical mass of useful data on possible nanoadditives for e-fluids. The development of e-fluids based on stable nanoadditives requires a deeper knowledge of the relationships between their chemical nature, their thermophysical and transport properties, and their tribological interaction with different solid surfaces. In this fundamental work, the effect of the size of two commercial Fe_3O_4 NPs modified with a silane, octadecyltrichlorosilane (OTS), on these parameters was first investigated. Such fundamental studies are necessary, but the combinations are enormous and not all of them can be studied experimentally under all conditions. Recently, the field of tribology has experienced significant developments in both scope and depth and, as a result, information from tribology research has been accumulating rapidly [57]. Another problem is that not all studies report the results in a comparable way. For example, many studies lack information on the stability of nanodispersions over time, which is crucial data as a starting point for gaining knowledge about reliable nanoadditives that could be used in real-world applications. Another drawback is that the different experimental conditions between tests performed by different researchers make it extremely difficult to compare the tribological results, as they are significantly affected by the experimental conditions. Standard measurements should be considered to improve the quality of the results from a global perspective. At the same time, computational technology has developed rapidly and has proven to be an efficient and reliable method for reducing the entropy of tribological information [57]. Thus, Tribo-informatics is emerging as an interdisciplinary field combining tribology and Computer Science, giving new impetus and added value to tribological research [58].

CRediT authorship contribution statement

Fátima Mariño: Writing – review & editing, Writing – original draft, Methodology, Investigation, Conceptualization. **Óscar Giner-Rajala:** Writing – review & editing, Methodology, Investigation. **Enriqueta R. López:** Writing – review & editing, Validation, Supervision, Formal analysis, Conceptualization. **Alfredo Amigo:** Writing – review & editing, Validation, Supervision, Formal analysis, Conceptualization. **Josefa Fernández:** Writing – review & editing, Validation, Supervision, Project administration, Funding acquisition, Conceptualization.

Declaration of competing interest

The authors declare that they have no known competing financial interests or personal relationships that could have appeared to influence the work reported in this paper.

Acknowledgments

The authors thank Repsol Lubricants for providing the PAO6 base oil and RIAIDT-USC for its analytical facilities. This research was funded by Xunta de Galicia (ED431C 2024/06) and by MCIN/AEI/10.13039/501100011033 though the PID2020-112846RB-C22 project.

Data availability

Data will be made available on request.

References

[1] D. Berman, L. Farfan-Cabrera, A. Rosenkranz, A. Erdemir, 2D materials for durable and sustainable electric vehicles, Nat. Rev. Mater. (2024), https://doi.org/10.1038/s41578-024-00680-3.
[2] W.A.A. Mustafa, F. Dassenoy, M. Sarno, A. Senatore, A review on potentials and challenges of nanolubricants as promising lubricants for electric vehicles, Lubr. Sci. 34 (2022) 1–29, https://doi.org/10.1002/ls.1568.
[3] Perspective on Electric Vehicles. 2019 Annual Report Lubes'n'Greases, LNG Publishing Company; Inc, USA, 2019, pp. 23–27.
[4] N. McGuire, The brave new world of electric vehicle fluids, Tribol. Lubr. Technol. 77 (10) (2021) 30–38.
[5] A. Gangopadhyay, N. Jost, K.C. Mutyala. 10 - Lubrication regimes in battery electric vehicle power unit, in: Electric Vehicle Tribology. L.I. Farfan-Cabrera, A. Erdemir, eds. Elsevier, 2024, pp. 183–191. ISBN: 9780443140747.
[6] N. Canter, Heat transfer fluids: growing in visibility and importance, Tribol. Lubr. Technol. 77 (12) (2021) 28–40.
[7] H. Kumar, A.P. Harsha. 11 - Group IV Base Stock. In: Tribology and Sustainability. J.K. Katiyar, M.I.U. Haq, A. Raina, S. Jayalakshmi, R. Arvind Singh, eds. CRC Press; 2021, pp. 163–188. ISBN: 9781003092162.
[8] Z. Guan, Z. Wu, J. Liu, X. Tu, S. Li, Controllable fabrication of magnesium silicate hydroxide reinforced MoS_2 hybrid nanomaterials as effective lubricant additives in PAO, Appl. Surf. Sci. 597 (2022) 153777, https://doi.org/10.1016/j.apsusc.2022.153777.
[9] B. Jin, J. Zhao, G. Chen, Y. He, Y. Huang, J. Luo, In situ synthesis of Mn_3O_4/graphene nanocomposite and its application as a lubrication additive at high temperatures, Appl. Surf. Sci. 546 (2021) 149019, https://doi.org/10.1016/j.apsusc.2021.149019.
[10] J. Siregar, N.L.W. Septiani, S.A. Abrori, K. Sebayang, H. Irzaman, M.Z. Fahmi, S. Humaidi, T. Sembiring, K. Sembiring, B. Yuliarto, Review—a pollutant gas sensor based on Fe_3O_4 nanostructures: a review, J. Electrochem. Soc. 168 (2021) 027510, https://doi.org/10.1149/1945-7111/abd928.
[11] Y.P. Yew, K. Shameli, M. Miyake, N.B.B. Ahmad Khairudin, S.E.B. Mohamad, T. Naiki, K.X. Lee, Green biosynthesis of superparamagnetic magnetite Fe_3O_4 nanoparticles and biomedical applications in targeted anticancer drug delivery system: a review, Arab. J. Chem. 13 (2020) 2287–2308, https://doi.org/10.1016/j.arabjc.2018.04.013.
[12] M.D. Nguyen, H. Tran, S. Xu, T.R. Lee, Fe_3O_4 nanoparticles: structures, synthesis, magnetic properties, surface functionalization, and emerging applications, Appl. Sci. 11 (2021) 11301, https://doi.org/10.3390/app112311301.
[13] L.R. de Oliveira, T.A. Rodrigues, H.L. Costa, W.M. da Silva Jr, Scuffing resistance of polyalphaolefin (PAO)-based nanolubricants with oleic acid (OA) and iron oxide nanoparticles, Mater. Today Commun. 31 (2022) 103837, https://doi.org/10.1016/j.mtcomm.2022.103837.
[14] A. Zuin, T. Cousseau, A. Sinatora, S.H. Toma, K. Araki, H.E. Toma, Lipophilic magnetite nanoparticles coated with stearic acid: a potential agent for friction and wear reduction, Tribol. Int. 112 (2017) 10–19, https://doi.org/10.1016/j.triboint.2017.03.028.
[15] W. Huang, X. Wang, G. Ma, C. Shen, Study on the synthesis and tribological property of Fe_3O_4 based magnetic fluids, Tribol. Lett. 33 (2009) 187–192, https://doi.org/10.1007/s11249-008-9407-1.
[16] J.M. Liñeira del Río, E.R. López, M. González Gómez, S. Yáñez Vilar, Y. Piñeiro, J. Rivas, D.E.P. Gonçalves, J.H.O. Seabra, J. Fernández, Tribological behavior of nanolubricants based on coated magnetic nanoparticles and trimethylolpropane trioleate base oil, Nanomaterials 10 (2020) 683, https://doi.org/10.3390/nano10040683.
[17] M.J.G. Guimarey, J.M. Liñeira del Río, J. Fernández, Improvement of the lubrication performance of an ester base oil with coated ferrite nanoadditives for different material pairs, J. Mol. Liq. 350 (2022) 118550, https://doi.org/10.1016/j.molliq.2022.118550.
[18] G. Zhou, Y. Zhu, X. Wang, M. Xia, Y. Zhang, H. Ding, Sliding tribological properties of 0.45% carbon steel lubricated with fe_3o_4 magnetic nano-particle additives in baseoil, Wear 301 (2013) 753–757, https://doi.org/10.1016/j.wear.2013.01.027.
[19] C. Gao, Y. Wang, D. Hu, Z. Pan, L. Xiang, Tribological properties of magnetite nanoparticles with various morphologies as lubricating additives, J. Nanopart. Res. 15 (2013) 1502, https://doi.org/10.1007/s11051-013-1502-z.
[20] C. Shen, W. Huang, G. Ma, X. Wang, A novel surface texture for magnetic fluid lubrication, Surf. Coat. Technol. 204 (2009) 433–439, https://doi.org/10.1016/j.surfcoat.2009.08.003.
[21] B.L. Prajapati, Magnetic-fluid-based porous squeeze films, J. Magn. Magn. Mater. 149 (1995) 97–100, https://doi.org/10.1016/0304-8853(95)00346-0.
[22] M.J.G. Guimarey, M.J.P. Comuñas, E.R. López, A. Amigo, J. Fernández, Thermophysical properties of polyalphaolefin oil modified with nanoadditives, J. Chem. Thermodyn. 131 (2019) 192–205, https://doi.org/10.1016/j.jct.2018.10.035.
[23] N.F. Azman, S. Samion, Dispersion stability and lubrication mechanism of nanolubricants: a review, Int. J. Precis. Eng. Man-GT. 6 (2019) 393–414, https://doi.org/10.1007/s40684-019-00080-x.
[24] K.H. Lee, H.R. Cha, Y.B. Kim, Development of an interior permanent magnet motor through rotor cooling for electric vehicles, Appl. Therm. Eng. 95 (2016) 348–356, https://doi.org/10.1016/j.applthermaleng.2015.11.022.
[25] K. Arole, M.J. Green, H. Liang. 11 - Thermal and electrical properties of electric vehicle fluids, in: Electric Vehicle Tribology. L.I. Farfan-Cabrera, A. Erdemir, eds. Elsevier, 2024, pp. 193–206. ISBN: 9780443140747.
[26] G. Socrates, Infrared and Raman Characteristic Group Frequencies: Tables and Charts, John Wiley & Sons, 2004.
[27] F. Yaghoubidoust, E. Salimi, Antibacterial and antiplatelet properties of octyltrichlorosilane-modified cotton fabrics, Fiber. Polym. 20 (2019) 1375–1379, https://doi.org/10.1007/s12221-019-1111-2.
[28] A. Kumar, J. Richter, J. Tywoniak, P. Hajek, S. Adamopoulos, U. Šegedin, M. Petrič, Surface modification of norway spruce wood by octadecyltrichlorosilane (OTS) nanosol by dipping and water vapour diffusion properties of the OTS-modified wood, Holzforschung 72 (2017) 45–56, https://doi.org/10.1515/hf-2017-0087.
[29] S. Chandrasekaran, R. Castaing, A. Cruz-Izquierdo, J.L. Scott, Influence of calcium silicate and hydrophobic agent coatings on thermal, water barrier, mechanical and biodegradation properties of cellulose, Nanomaterials 11 (2021) 1488, https://doi.org/10.3390/nano11061488.
[30] A.M. Kansara, V.K. Aswal, P.S. Singh, Preparation and characterization of new poly (dimethylsiloxane) membrane series via a 'cross-linking' reaction using monomolecular trichloro(alkyl)silane of different alkyl chain and type, RSC Adv. 5 (2015) 51608–51620, https://doi.org/10.1039/C5RA06433C.
[31] J.D. Presilla-Márquez, C.M.L. Rittby, W.R.M. Graham, Vibrational Spectra of hexa-atomic silicon-carbon clusters. I. Linear SiC_4Si, J. Chem. Phys. 106 (1997) 8367–8373, https://doi.org/10.1063/1.473898.
[32] K. Yang, H. Peng, Y. Wen, N. Li, Re-examination of characteristic FTIR spectrum of secondary layer in bilayer oleic acid-coated Fe_3O_4 nanoparticles, Appl. Surf. Sci. 256 (2010) 3093–3097, https://doi.org/10.1016/j.apsusc.2009.11.079.
[33] L. Slavov, M.V. Abrashev, T. Merodiiska, C. Gelev, R.E. Vandenberghe, I. Markova-Deneva, I. Nedkov, Raman spectroscopy investigation of magnetite nanoparticles in ferrofluids, J. Magn. Magn. Mater. 322 (2010) 1904–1911, https://doi.org/10.1016/j.jmmm.2010.01.005.
[34] Y. Chen, P. Renner, H. Liang, Dispersion of nanoparticles in lubricating oil: a critical review, Lubricants 7 (2019), https://doi.org/10.3390/lubricants7010007.
[35] H. Cao, J. He, L. Deng, X. Gao, Fabrication of cyclodextrin-functionalized superparamagnetic Fe_3O_4/amino-silane core–shell nanoparticles via layer-by-layer method, Appl. Surf. Sci. 255 (2009) 7974–7980, https://doi.org/10.1016/j.apsusc.2009.04.199.
[36] B. Feng, R.Y. Hong, L.S. Wang, L. Guo, H.Z. Li, J. Ding, Y. Zheng, D.G. Wei, Synthesis of Fe_3O_4/APTES/PEG diacid functionalized magnetic nanoparticles for MR imaging, Colloids Surf. Physicochem. Eng. Aspects 328 (2008) 52–59, https://doi.org/10.1016/j.colsurfa.2008.06.024.
[37] M.A. Legodi, D. de Waal, The preparation of magnetite, goethite, hematite and maghemite of pigment quality from mill scale iron waste, Dyes Pigment. 74 (2007) 161–168, https://doi.org/10.1016/j.dyepig.2006.01.038.
[38] K.G. Brown, E. Bicknell-Brown, M. Ladjadj, Raman-active bands sensitive to motion and conformation at the chain termini and backbones of alkanes and lipids, J. Phys. Chem. 91 (1987) 3436–3442, https://doi.org/10.1021/j100296a066.
[39] W.R. Thompson, J.E. Pemberton, Characterization of octadecylsilane and stearic acid layers on Al_2O_3 surfaces by raman spectroscopy, Langmuir 11 (1995) 1720–1725, https://doi.org/10.1021/la00005a048.
[40] M. Iijima, M. Tsukada, H. Kamiya, Effect of particle size on surface modification of silica nanoparticles by using silane coupling agents and their dispersion stability in

methylethylketone, J. Colloid Interface Sci. 307 (2007) 418–424, https://doi.org/10.1016/j.jcis.2006.11.044.
[41] J.M. Liñeira del Río, R. Rial, E.R. López, J. Fernández, Tribological enhancement using Mn_3O_4-graphene nanocomposites as additives for potential transmission fluids of electric vehicles, J. Mol. Liq. 366 (2022) 120271, https://doi.org/10.1016/j.molliq.2022.120271.
[42] J.M. Liñeira del Río, E.R. López, J. Fernández, Tribological behavior of electric vehicle transmission oils using Al_2O_3 nanoadditives, J. Mol. Liq. 397 (2024) 124036, https://doi.org/10.1016/j.molliq.2024.124036.
[43] B. Wang, F. Qiu, G.C. Barber, Q. Zou, J. Wang, S. Guo, Y. Yuan, Q. Jiang, Role of nano-sized materials as lubricant additives in friction and wear reduction: a review, Wear 490–491 (2022) 204206, https://doi.org/10.1016/j.wear.2021.204206.
[44] F. Mariño, J.M. Liñeira del Río, D.E.P. Gonçalves, J.H.O. Seabra, E.R. López, J. Fernández, Effect of the addition of coated SiO_2 nanoparticles on the tribological behavior of a low-viscosity polyalphaolefin base oil, Wear 530–531 (2023) 205025, https://doi.org/10.1016/j.wear.2023.205025.
[45] O.Z. Sharaf, R.A. Taylor, E. Abu-Nada, On the colloidal and chemical stability of solar nanofluids: from nanoscale interactions to recent advances, Phys. Rep. 867 (2020) 1–84, https://doi.org/10.1016/j.physrep.2020.04.005.
[46] S. Shrestha, B. Wang, P. Dutta, Nanoparticle processing: understanding and controlling aggregation, Adv. Colloid Interface Sci. 279 (2020) 102162, https://doi.org/10.1016/j.cis.2020.102162.
[47] F. Mariño, J.M. Liñeira del Río, E.R. López, J. Fernández, Chemically modified nanomaterials as lubricant additive: time stability, friction, and wear, J. Mol. Liq. 382 (2023) 121913, https://doi.org/10.1016/j.molliq.2023.121913.
[48] M. Ratoi, H. Tanaka, B.G. Mellor, J. Sugimura, Hydrocarbon lubricants can control hydrogen embrittlement, Sci. Rep. 10 (2020) 1361, https://doi.org/10.1038/s41598-020-58294-y.
[49] K.I. Nasser, J.M. Liñeira del Río, E.R. López, J. Fernández, Synergistic effects of hexagonal boron nitride nanoparticles and phosphonium ionic liquids as hybrid lubricant additives, J. Mol. Liq. 311 (2020) 113343, https://doi.org/10.1016/j.molliq.2020.113343.
[50] K.I. Nasser, J.M. Liñeira del Río, E.R. López, J. Fernández, Hybrid combinations of graphene nanoplatelets and phosphonium ionic liquids as lubricant additives for a polyalphaolefin, J. Mol. Liq. 336 (2021) 116266, https://doi.org/10.1016/j.molliq.2021.116266.
[51] L. Zhang, L. Chen, H. Wan, J. Chen, H. Zhou, Synthesis and tribological properties of stearic acid-modified anatase (TiO_2) nanoparticles, Tribol. Lett. 41 (2011) 409–416, https://doi.org/10.1007/s11249-010-9724-z.
[52] A. Banerji, M.J. Lukitsch, B. McClory, D.R. White, A.T. Alpas, Effect of iron oxides on sliding friction of thermally sprayed 1010 steel coated cylinder bores, Wear 376–377 (2017) 858–868, https://doi.org/10.1016/j.wear.2017.02.032.
[53] J. Van Rensselar, Rapidly expanding electric vehicle market spurs lubricant development urgency, Tribol. Lubr. Technol. 78 (11) (2022) 34–40.
[54] S. Mishra, M. Nayak, A. Misra. Thermal conductivity of nanofluids-a comprehensive review. Int. J. Thermofluid Sci. Technol. 7 (2020) 070301. doi: 10.36963/IJTST.2020070301.
[55] P.M. Martínez-Rubio, M.D. Avilés, J. Arias-Pardilla, F.J. Carrión-Vilches, J. Sanes, M.D. Bermúdez, R. Pamies, Physicochemical characterisation of graphene-ammonium lactate ionic liquid nanofluid, J. Mol. Liq. 367 (2022) 120446, https://doi.org/10.1016/j.molliq.2022.120446.
[56] J.M. Liñeira del Río, E.R. López, F. García, J. Fernández, Tribological synergies among chemical-modified graphene oxide nanomaterials and a phosphonium ionic liquid as additives of a biolubricant, J. Mol. Liq. 336 (2021) 116885, https://doi.org/10.1016/j.molliq.2021.116885.
[57] Z. Zhang, N. Yin, S. Chen, C. Liu, Tribo-informatics: concept, architecture, and case study, Friction 9 (2021) 642–655, https://doi.org/10.1007/s40544-020-0457-3.
[58] N. Yin, P. Yang, S. Liu, S. Pan, Z. Zhang, AI for tribology: present and future, Friction 12 (2024) 1060–1097, https://doi.org/10.1007/s40544-024-0879-2.